Energy gap variation due to Al content in $SmFe_{1-x}Al_xO_3$ and its application in optics

Ahmed Mohamed Fawzy[1] ✉, *Ashraf Kamal Eessaa*[1], *Yasser A. Saeid*[2]

[1]*Nanotechnology Central Lab, Electronics Research Institute, El Tahrir St., Giza, 12622, Egypt*
[2]*Department of Physics and Mathematics, NewCairo Academy, Higher Institute of Engineering and Technology, Cairo, Egypt*
✉ *E-mail: ahmed.fawzy.1986@ieee.org*

Published in Micro & Nano Letters; Received on 25th May 2018; Revised on 6th August 2018; Accepted on 24th September 2018

The optical properties of Al-doped $SmFeO_3$ ($SmFe_{1-x}Al_xO_3$, for x varying from 0 to 0.15), were monitored by diffuse reflectance spectroscopy (DRS). The diffuse reflectance spectra were used to study the surface properties of the samples. The DRS spectra exhibit three reflection bands at different regions. The product was characterised by X-ray diffraction to confirm the formation of single-phase crystals of the perovskite structure. The bandgap, a major factor in determining the optical performance of any material, was found to be tunable with Al content (x).

1. Introduction: The optical bandgap (E_g) is explained as the minimum energy required to move an electron from the valence band to the conduction band. In a pure, undoped crystal the optical gap is equal to the energy separation (E_{g0}) between the conduction band edge and the valence band edge. The optical and electronic properties of semiconductor materials can be characterised by using the energy gap because of the relation between the refractive index and the energy gap. The nature and magnitude of the energy gap and refractive index are used to determine the applications of semiconductors as optoelectronic and optical devices. The performance assessment of the bandgap engineered structures depends on these properties for continuous and optimal absorption of broadband spectral sources. A prior knowledge of the refractive index and energy gap is required to deal with different devices such as solar cells, waveguides, detectors, and photonic crystals. Coating technologies rely on the spectral properties of materials. These technologies include antireflection coatings and optical filters [1]. The threshold for absorption of photons in a semiconductor can be determined by energy gap and the refractive index is a measure of its transparency to incident spectral radiation. The relation between these two significant properties has a great effect on the band structure of semiconductors [2]. In 1950, Moss proposed the following basic relationship between these two properties using the general theory of photoconductivity, which was based on the photo effect [2, 3]

$$n^4/\lambda_e = 77/\mu\text{m} \tag{1}$$

where n is the refractive index and λ_e is the wavelength corresponding to the absorption edge. In terms of the energy gap, this expression is [4]

$$n^4 E_g = 95\,\text{eV} \tag{2}$$

According to this relation, the refractive index of a semiconductor can be determined with a known energy gap. Therefore, the study of the energy gap is very important for determining the performance of any material.

In this Letter, Al is exploited to control or alter the bandgap of a material. This process named bandgap engineering. Layered materials with alternating compositions can be constructed by different techniques such as molecular beam epitaxy. These methods are exploited in the design of laser diodes.

Rare-earth perovskite orthoferrites present interesting properties and are studied for their potential applications in microelectronics, bioengineering, and smart devices and for their meeting the requirement of miniaturisation and low-power consumption in such electronic components [5]. Understanding the crystallisation mechanisms and characterising such perovskites are thus important for understanding their properties. Induced modifications in different functional properties (such as magnetic and optical) of $SmFeO_3$ can be achieved by introducing intended magnetic vacancies into the Fe sublattice by substitution of non-magnetic ions that can produce additional anisotropy in the rare-earth orthoferrite system. Because dilution effects cannot be neglected even in a small concentration of vacancies, their relevance strongly depends on the nature of the rare-earth ion [6].

Herein, we emphasise the influence of the variation of the B site cation radius by substituting Fe^{+3} ions with Al^{+3} ions. The physical properties of a series of $SmFe_{1-x}Al_xO_3$ compounds, where $0.0 \le x \le 0.15$ in steps of 0.05, are explored to discover novel characterisations and to open a new era of optical applications. The tuning of Al composition (x) will lead to changes in optical properties [7–9].

In this Letter, the crystal structure and microstructure of ($SmFe_{1-x}Al_xO_3$, for x varying from 0 to 0.15) are explored and shows the influence of Al^{+3} ions content (x) by using X-ray diffraction (XRD). XRD helps us to investigate the structural variations of the unit cell of $SmFeO_3$ parent compound upon the substitution with Al^{+3} ions. Fig. 1 illustrates the XRD pattern for the samples ($SmFe_{1-x}Al_xO_3$, for x varying from 0 to 0.15). The analysis of the XRD pattern reveals the formation of the structure. The data were compared and indexed with reference ICDD card no. 04-006-8304. The intensity of the diffraction lines depends slightly on the Al^{+3} content in the orthoferrite lattice. Al^{+3} content (x) was limited at the value of 0.15 due to the appearance of the secondary phase, which means the material has another component indexed as Al_2O_3 with relatively small intensities.

In this study, we propose a detailed explanation of the optical properties of orthoferrites and we investigate the optical properties by using diffuse reflectance spectroscopy (DRS) measurements. The Letter is organised as follows: In Section 2, the materials and fabrication method are explained in detail. In Section 3, results and discussion are explained and we show the DRS concept and the results that show how the energy gap is affected by Al concentration. In Section 4, we present our conclusions.

2. Materials and methods: Double sintering ceramic technology was used to prepare samples of $SmFe_{1-x}Al_xO_3$ with different concentrations of Al, from 0 to 0.15 in steps of 0.05. Analar grade oxides (Sm_2O_3, Al_2O_3, and Fe_2O_3) were mixed together. The preparation consisted of four steps:

doi: 10.1049/mnl.2018.5216

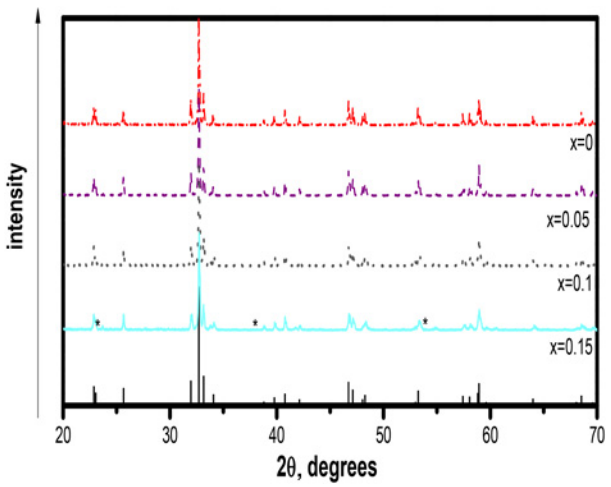

Fig. 1 *XRD patterns of the samples ($SmFe_{1-x}Al_xO_3$, for x varying from 0 to 0.15) *Secondary phase*

1. Stoichiometric ratios were well mixed.
2. Grinding and pre-sintering were done at a certain rate.
3. Regrinding and final sintering were done at a certain rate.
4. The samples were pressed into pellets.

The detailed description of the preparation is presented in Fig. 2.

3. Results and discussion: The optical range from ultraviolet (UV), though visible (vis), to infrared (IR) was characterised by using DRS, in which a Varian 5E spectrometer with a $BaSO_4$-coated integration sphere was used. DRS is a technique in which scattered energy is collected and analysed. The sample is projected to the beam which reflects off the surface of the particle or be transmitted through a particle. The energy reflecting off the surface is typically lost. The beam that passes through a particle can either reflect off the next particle or be transmitted through the next particle. These transmission and reflectance events can occur many times in the sample, which increases the path length. Finally, the scattered energy is collected by a spherical mirror that is focused onto the detector. The detected light is partially absorbed by particles of the sample, yielding the sample information as shown in Fig. 3. There are two techniques for the measurement, either the single-beam or the double-beam arrangements. In the single-beam arrangement, the value of primary beam intensity is recorded prior to the measurement. Its disadvantage is the temperature dependence of the electronic detection system, so all measurements must be taken in constant temperature rooms. In double-beam arrangement, the primary beam splits into the sample beam and reflectance beam. The arrangements avoid any effect due to the experimental environment.

DRS has many advantages than other techniques. It is a simple method of investigation, a suitable and non-destructive. These advantages are important in examinations of gels, porous and nano-crystalline materials. It is impossible to examine such materials by using traditional methods of investigation and it is also difficult to determine the path length in optical transmittance through them. The high spectral quality of diffuse reflectance relates to the following factors: (i) the sample must be diluted with a non-absorbing matrix to ensure a deeper penetration of the incident beam into the sample, which decreases the specular reflection component and maximises the contribution of the scattered component

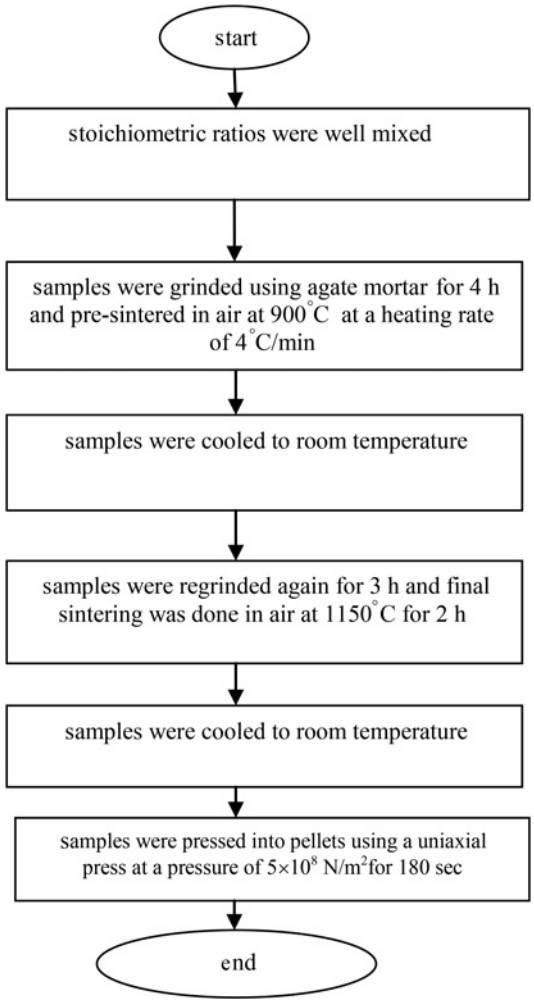

Fig. 2 *Flowchart describing the preparation method of $SmFe_{1-x}Al_xO_3$, where x varies from 0 to 0.15 in steps of 0.05*

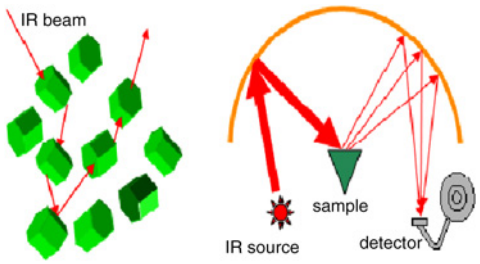

Fig. 3 *Schematic diagram of DRS*

in the spectrum, and (ii) the quality of DRS spectra is improved by smaller particles.

In this Letter, the surface structure of $SmFe_{1-x}Al_xO_3$ pellets was probed by UV–vis–IR diffuse reflectance spectroscopy. Fig. 4 shows the DRS spectra of x varying from 0 to 0.15. If $x = 0$, there is no Al. It is clear that there are several reflection bands within the three reflection regions: UV, vis, and IR. There are several absorption bands in the UV region centred around 228, 240, 300, and 320 nm. In the visible range (400–800) nm, there is mainly one absorption band peaked at ~622 nm, with an absorption edge at ~470 nm.

The optical bandgap can be determined from DRS measurements [10, 11]. In a diffuse reflectance spectrum, the ratio of the light scattered from a thick layer of the sample to that from an ideal

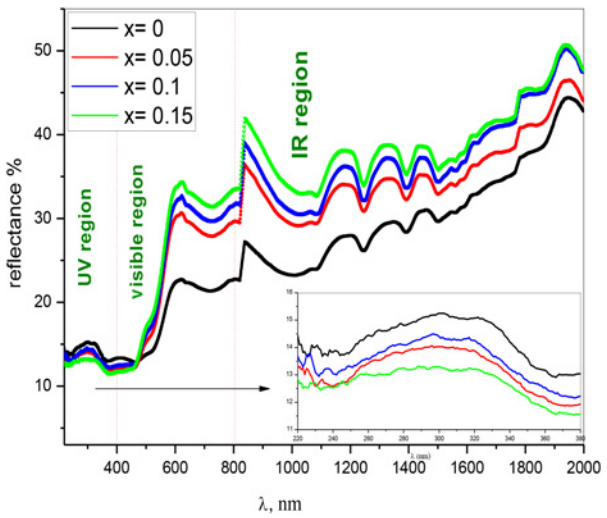

Fig. 4 *UV–vis–IR diffuse reflectance spectra*

non-absorbing reference sample is measured as a function of the wavelength by using the Schuster–Kubelka–Munk (SKM) remission function (i.e. FSKM(R_∞) versus l in nanometres) [12–15]. Kubelka–Munk theory was used for the analysis of the diffuse reflectance spectra, as expressed by the following equation:

$$\mathrm{FSKM}(R_\infty) = (1 - R_\infty)2/2R_\infty = K/S. \tag{3}$$

The relation among the diffuse reflectance of the sample (R_∞) and absorption (K) and scattering (S) coefficients are related by the SKM remission function. The SKM remission function relates the experimentally determined diffuse reflectance of a thick sample to K and S. The limiting fraction of the absorption of light per unit thickness is called the absorption coefficient. The limiting fraction of the light energy scattered backward per unit thickness, as thickness tends to zero is called the scattering coefficient. At constant S, FSKM(R_∞) is directly proportional to K, and a plot of FSKM (R_∞) vs concentration of the absorbing species should be a straight line passing through the origin. This linear relationship can be used for quantitative studies of powder samples of infinite layer thickness containing uniformly distributed metal ions in low concentration. DRS has been used extensively to study transition metal oxides to obtain information on surface coordination and different oxidation states of metal ions. However, this technique has limitations owing to the difficulty in interpreting the large bandwidths and specular reflectance often observed in the spectra.

The bandgap energies of $SmFe_{1-x}Al_xO_3$ were evaluated from optical reflectance spectra by extrapolating the straight line plot of $(F(R_\infty)h\nu)^2$ versus $h\nu$ according to the following Kubelka–Munk equation as shown in Fig. 5 [16]:

$$F(R_\infty) = A(h\nu - E_g)^n \tag{4}$$

where h is Planck's constant, ν is the frequency of vibration, E_g is the bandgap, and A is a proportional constant. The value of the exponent n denotes the nature of the sample transition: $n = 1/2$ for a direct allowed transition, $n = 3/2$ for a direct forbidden transition, $n = 2$ for an indirect allowed transition, and $n = 3$ for an indirect forbidden transition. Because the direct allowed transition is used in this experiment, $n = 1/2$ is used for these samples. The obtained bandgap of $SmFe_{1-x}Al_xO_3$ versus Al composition (x) is plotted in Fig. 6. One can see that the bandgap value decreases with increasing Al content (x). It is clear that the resulting bandgap energies are large (wide). The bandgap energies of materials are related to the wavelength that is generated from the light source [17–19].

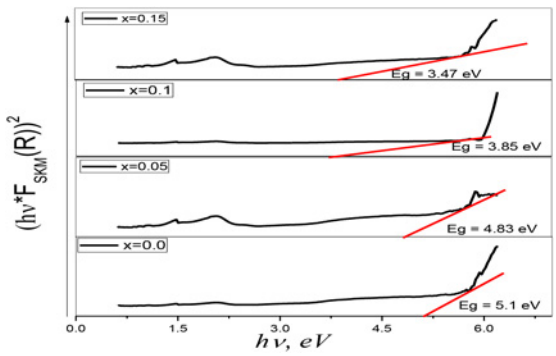

Fig. 5 *$h\nu F_{SKM}(R))^2$ versus hν graphs for $SmFe_{1-x}Al_xO_3$ (x = 0.0, 0.05, 0.1, and 0.15) system*

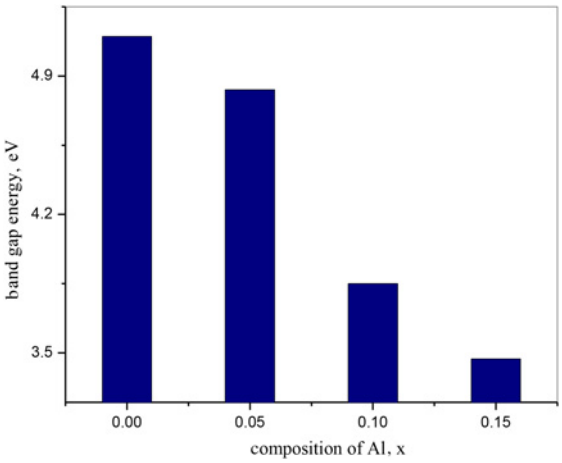

Fig. 6 *Variations of the energy gap of $SmFe_{1-x}Al_xO_3$ when x is varied from 0 to 0.15 in steps of 0.05*

Therefore, we recommend using the investigated system in light source applications.

4. Conclusion: We investigated the novel properties of Al-doped $SmFeO_3$ ($SmFe_{1-x}Al_xO_3$, where $0.0 \le x \le 0.15$ in steps of 0.05). Double sintering ceramic technology was used to synthesise the materials. On the basis of diffuse reflectance spectra, the optical bandgap of $SmFe_{1-x}Al_xO_3$ was determined and it was found that it can be tuned by altering the Al doping concentration (x). The wide bandgap that was determined by reflectance indicates that the system could be useful in optical applications, especially for light sources.

5 References

[1] Tong F.M., Ravindra N.M., Kosonocky W.F.: 'Design and simulation of permissible tolerance during fabrication of infrared-induced transmission filters', *Opt. Eng.*, 1997, **36**, (2), pp. 549–558

[2] Ravindra N.M., Ganapathy P., Choi J.: 'Energy gap–refractive index relations in semiconductors – an overview', *Infrared Phys. Technol.*, 2007, **50**, (1), pp. 21–29

[3] Moss T.S.: 'Photoconductivity in the elements' (Academic, New York, 1952)

[4] Moss T.S.: 'Relations between the refractive index and energy gap of semiconductors', *Phys. Status Solidi B*, 1985, **131**, (2), pp. 415–427

[5] Li N.N., Li Y., Li H., *ET AL.*: 'Doping effects on structural and magnetic evolutions of orthoferrite $SmFe_{1-x}Al_xO_3$', *Chin. Phys. B*, 2014, **23**, (6), p. 069101

[6] Lee J.H., Jeong Y.K., Park J.H., *ET AL.*: 'Spin-canting-induced improper ferroelectricity and spontaneous magnetization reversal in $SmFeO_3$', *Phys. Rev. Lett.*, 2011, **107**, (11), p. 117201

doi: 10.1049/mnl.2018.5216

[7] Kulkarni S.A., Baikie T., Boix P.P., *ET AL.*: 'Band-gap tuning of lead halide perovskites using a sequential deposition process', *J. Mater. Chem. A*, 2014, **2**, (24), pp. 9221–9225
[8] Prasanna R., Gold-Parker A., Leijtens T., *ET AL.*: 'Band gap tuning via lattice contraction and octahedral tilting in perovskite materials for photovoltaics', *J. Am. Chem. Soc.*, 2017, **139**, (32), pp. 11117–11124
[9] Bush K.A., Frohna K., Prasanna R., *ET AL.*: 'Compositional engineering for efficient wide band gap perovskites with improved stability to photoinduced phase segregation', *ACS Energy Lett.*, 2018, **3**, (2), pp. 428–435
[10] Nowak M., Kauch B., Szperlich P.: 'Determination of energy band gap of nanocrystalline SbSI using diffuse reflectance spectroscopy', *Rev. Sci. Instrum.*, 2009, **80**, (4), p. 046107
[11] Zhang M., An T., Hu X., *ET AL.*: 'Preparation and photocatalytic properties of a nanometer ZnO–SnO_2 coupled oxide', *Appl. Catal. A, Gen.*, 2004, **260**, (2), pp. 215–222
[12] Rao G.R., Ranjan Sahu H.: 'XRD and UV-Vis diffuse reflectance analysis of CeO_2-ZrO_2 solid solutions synthesized by combustion method', *J. Chem. Sci.*, 2001, **113**, (5), pp. 651–658
[13] Ganjkhanlou Y., Crocellà V., Kazemzad M., *ET AL.*: 'Hydrothermal–electrochemical deposition of semiconductor thin films: the case of CuIn (Al) Se2 compound', *J. Mater. Sci., Mater. Electron.*, 2017, **28**, (20), pp. 15596–15604
[14] Bulánek R., Čičmanec P., Setnička M.: 'Possibility of VOx/SiO_2 complexes speciation: comparative multi-wavelength Raman and DR UV-vis study', *Phys. Proc.*, 2013, **44**, pp. 195–205
[15] Ganjkhanlou Y., Tišler Z., Hidalgo J.M., *ET AL.*: 'VOx/Zr–SBA-15 catalysts for selective oxidation of ethanol to acetaldehyde', *Chem. Pap.*, 2018, **72**, (4), pp. 937–946
[16] Ahmed M.A., Dhahri E., El-Dek S.I., *ET AL.*: 'Size confinement and magnetization improvement by La3+ doping in $BiFeO_3$ quantum dots', *Solid State Sci.*, 2013, **20**, pp. 23–28
[17] Fawzy A., El-Ghandour O.M., Hamed H.F.A.: 'A dual cylindrical tunable laser based on MEMS', *Int. J. Adv. Comput. Sci. Appl.*, 2016, **1**, (7), pp. 128–132
[18] Fawzy A., Elghandour O., Hamed H.F.A.: 'Diffraction effects on a dual external cavity tunable laser ECTL source'. Progress in Electromagnetics Research Symp. (PIERS) Conf., Prague Czech Republic, 2015, pp. 6–9
[19] Fawzy A., El-Ghandour O.M., Hamed H.F.A.: 'Performance analysis on a dual external cavity tunable laser ECTL source', *J. Electromagn. Anal Appl.*, 2015, **7**, (4), p. 134